How to cite: *Angew. Chem. Int. Ed.* **2022,** *61,* e202208139
International Edition: doi.org/10.1002/anie.202208139
German Edition: doi.org/10.1002/ange.202208139

Metal-Organic Frameworks

Tetrazine Linkers as Plug-and-Play Tags for General Metal-Organic Framework Functionalization and C_{60} Conjugation

*Belén Lerma-Berlanga, Carolina R. Ganivet, Neyvis Almora-Barrios, Rebecca Vismara, Jorge A. R. Navarro, Sergio Tatay, Natalia M. Padial, and Carlos Martí-Gastaldo**

Dedicated to Nazario Martín on the occasion of his 66th birthday.

Abstract: The value of covalent post-synthetic modification in expanding the chemistry and pore versatility of reticular solids is well documented. Here we use mesoporous crystals of the metal–organic framework (MOF) UiO-68-TZDC to demonstrate the value of tetrazine connectors for all-purpose inverse electron-demand Diels–Alder ligation chemistry. Our results suggest a positive effect of tetrazine reticulation over its reactivity for quantitative one-step functionalization with a broad scope of alkene or alkyne dienophiles into pyridazine and dihydropyridazine frameworks. This permits generating multiple pore environments with diverse chemical functionalities and the expected accessible porosities, that is also extended to the synthesis of crystalline fulleretic materials by covalent conjugation of fullerene molecules.

Introduction

Post-synthetic modification (PSM) is a universal tool for functionalizing and expanding the pore chemistry of reticular solids as Metal-Organic Frameworks (MOFs) and Covalent Organic Frameworks (COFs).[1,2] The organic components in these networks offer appealing opportunities for the implementation of new chemical functionalities that are respectful with the original structure and in most cases not accessible by direct synthesis. This is for instance the case of nanocarbons as fullerene or nanographenes, whose functionalization and purification to obtain soluble linkers is quite laborious and time-consuming. Covalent PSM generally requires adequate chemical tags in the organic strut for covalent functionalization in presence of soluble reagents.[3] These tags have been traditionally restricted to amino or aldehyde groups for imine condensation,[4] acylation[5] alkylation[6] or conversion to hydrazones[7] to cite a few. The incorporation of azide or alkyne tags has been also central to the introduction of click chemistry to PSM. This route enables quantitative conjugation of a broad range of molecules by azide-alkyne 1,3-dipolar cycloaddition reactions under mild conditions in presence of Cu^{I} as catalyst.[8,9]

In this regard, the inverse Electron-Demand Diels–Alder (iEDDA) reaction between electron-poor dienes, as 1,2,4,5-tetrazines, and electron-rich dienophiles is an excellent alternative for metal-free click reactions. This reaction does not require a catalyst, offers fast kinetics, orthogonality with other click reactions, quantitative transformations under mild conditions, and inoffensive side products for minimum impact to the clicked frameworks.[10] iEDDA has been thoroughly studied in solution with particular focus on targeted synthesis of natural products[11] and bioconjugation reactions,[12] however, generic post-functionalization routes for MOFs are still missing. Precedents are based almost exclusively in the incorporation of dienophiles as olefins to amino-tagged MOFs for subsequent reaction with tetrazine.[13] This tandem approach requires two steps and is quite limiting in the scope of dienes accessible, thus limiting versatile engineering of pore chemistry. The alternative integration of dienes to the MOF structure would be arguably more adequate for all-purpose ligation chemistry but the number of candidates remains still very limited.[14–16] We recently reported the synthesis of UiO-68-TZDC crystals by reticulation of 4,4′-(1,2,4,5-tetrazine-3,6-diyl)dibenzoic acid (H_2tzdc) diene linkers into a mesoporous framework.[17] Here we present this tetrazine MOF as an ideal platform towards the generalization of iEDDA PSM chemistry for one-step functionalization with a broad scope of alkene/alkyne dienophiles to generate multiple pore environments with diverse chemical functionalities (Figure 1a). Our route can be also extended to the covalent conjugation of C_{60} molecules, that is directed by reaction with the tetrazine tags in the linker for the synthesis of porous, fulleretic crystals by precise positioning of the nanocarbons (Figure 1b).

[*] B. Lerma-Berlanga, Dr. C. R. Ganivet, Dr. N. Almora-Barrios, Dr. S. Tatay, Dr. N. M. Padial, Dr. C. Martí-Gastaldo
Functional Inorganic Materials Team, Instituto de Ciencia Molecular (ICMol), Universitat de València
Catedrático José Beltrán-2, 46980 Paterna (Spain)
E-mail: carlos.marti@uv.es
Dr. R. Vismara, Prof. J. A. R. Navarro
Departamento de Química Inorgánica, Universidad de Granada
Av. Fuentenueva S/N, 18071 Granada (Spain)

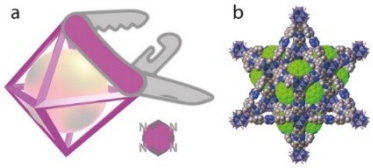

Figure 1. a) Use of tetrazine linkers as plug-and-play tags for general framework functionalization. b) Structure of UiO-68-TZDC(C_{60}) after one-step conjugation of fullerene molecules in green.

Results and Discussion

We initially used 2,5-norbornadiene (NBD) as model substrate to optimize the iEDDA reaction with UiO-68-TZDC (Figure 2a). We reacted the MOF crystals in different solvents (*N,N*-dimethylformamide, ether or acetonitrile) and variable temperatures (40, 60, 70 or 80 °C), reaction times (8 or 16 h), or dienophile equivalents per tetrazine linker (3:1 or 50:1), followed by thorough washing with ether and storage in hexane. According to the X-ray diffraction (PXRD) patterns of all samples, the best compromise between clean functionalization with negligible impact to the crystallinity of the framework was reached at 40 °C, with poor impact of the rest of parameters. Based on these tests, we selected reactions at 40 °C in ether stirring during 16 h in a shaker, with a 3:1 ratio as the optimum conditions. As shown in Figure 2a, the first step of the reaction involves a Diels–Alder [4+2] cycloaddition with inverse electron-demand resulting in a highly strained bicyclic adduct. Nevertheless, the distortion is mostly perpendicular to the long-axis of the ligand, thus preventing strain-induced disassembly of the MOF. This is also the case for tetrazine-edged supramolecular cages, as beautifully demonstrated by Nitschke and co-workers.[18] The initially formed adduct is then rapidly converted in a retro-Diels–Alder step (upon release of N_2) to the corresponding dihydropyridazine intermediate that spontaneously rearomatizes via a second retro-Diels–Alder reaction to eliminate a molecule of cyclopentadiene. In this case, NBD acts as an ethyne equivalent for the formation of pyridazine (PZDC). Quantitative formation of the PZDC MOF was confirmed by ^{1}H NMR of the crystals after digestion in D_2SO_4/DMSO-d_6 solutions. Figure 2b shows the appearance of the signal intrinsic to the pyridazine nucleus accompanied by the deshielding of the hydrogens in the aromatic rings adjacent to the PZDC core as result of the lower electron density. Despite the desymmetrization of the tetrazine linker, the spectrum shows the same pattern and multiplicity. Optical microscopy and SEM imaging (Figure S2) confirmed that the size and morphology of UiO-68-PZDC crystals are retained after the reaction. This is consistent with the negligible changes to unit cell parameters calculated by LeBail refinement of the PXRD patterns before and after the reaction (Figure 2c). iEDDA reaction yields a significant color change from pink to light yellow concomitant to the clean conversion of the tetrazine ring into pyridazine. Disappearance of the characteristic signal of tetrazine core was also confirmed by solid-state diffuse reflectance spectroscopy (Figure 3b). UiO-68-PZDC was solvent-exchanged with hexane and evacuated at 10^{-6} Torr overnight. It displays a non-hysteretic type-I N_2 isotherm with a multipoint BET surface area of near 4200 $m^2 g^{-1}$, almost coincident with the 4300 $m^2 g^{-1}$ displayed by pristine UiO-68-TZDC (Figure S3). Regarding stability in humid environments, UiO-68-PZDC shows higher chemical robustness than UiO-68-TZDC comparable to that of pristine UiO-68 (Figures S4 and S5) and we attribute these differences to the changes in polarity of the central ring for minimizing the interaction of the framework with polar solvents as water. As for the thermal decomposition profiles do not display significant changes in thermal stability (Figure S1).

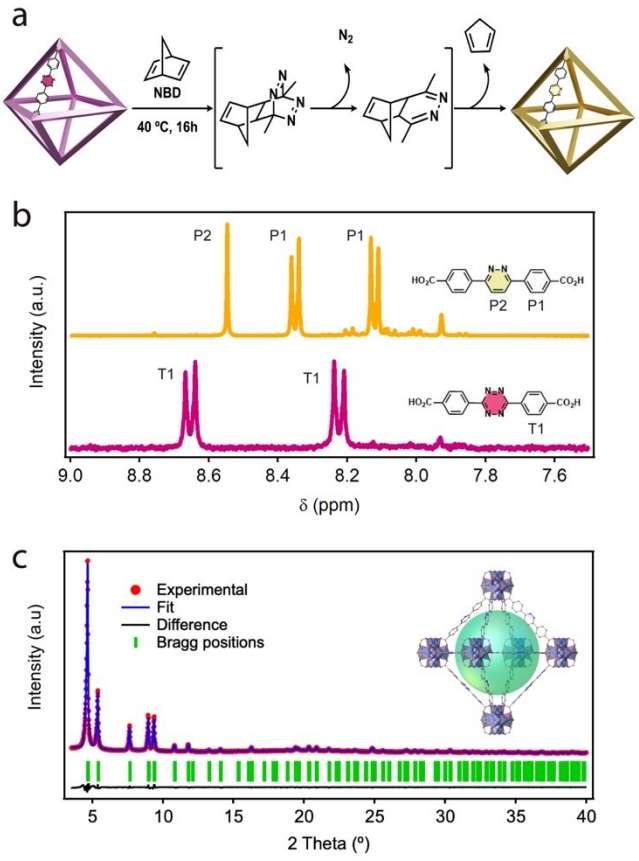

Figure 2. a) Mechanism of the iEDDA reaction between UiO-68-TZDC and NBD for post-synthetic modification of the framework. b) ^{1}H NMR spectra before/after reaction. c) PXRD LeBail refinement of UiO-68-PZDC. $Fm\bar{3}m$, $a=b=c=32.66080$ Å, $\alpha=\beta=\gamma=90°$, $R_p=3.04\%$, $R_{wp}=4.03\%$, $R_{exp}=2.47\%$, Chi2 = 2.66, GoF = 1.63.

For a better understanding of the effect of reticulating TZDC over iEDDA reactivity with NBD we monitored the reaction in controlled time intervals of up to 24 hours. Figure 3a shows the gradual change in color with time of the dispersions of UiO-68-TZDC crystals associated to the disappearance of the characteristic n→π* absorption band of the tetrazine ring at 558 nm. This change is consistent with the UV/Vis solid reflectance measurements of the MOF at variable times of reaction normalized to the

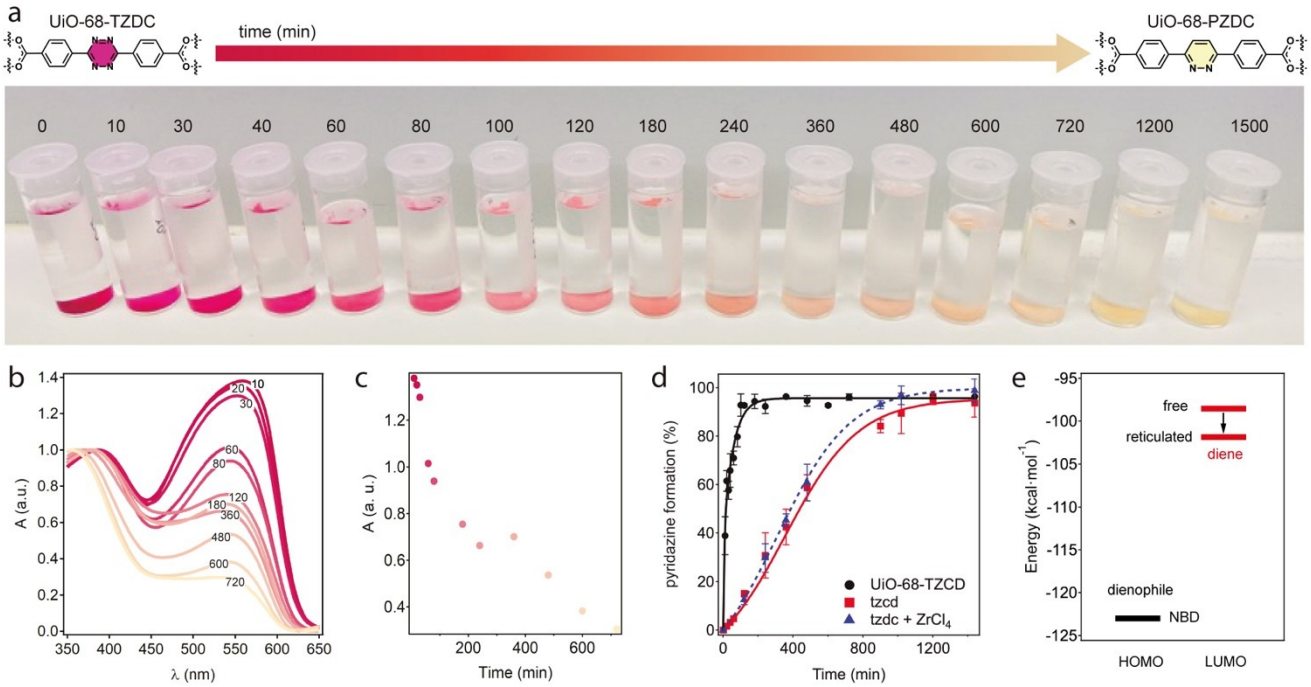

Figure 3. a) Progressive change in colour with time of UiO-68-TZDC crystals by iEDDA reaction with NBD in ether at 40 °C. b) Evolution of the UV/Vis diffuse reflectance spectra of the solid and c) decrease of intensity of the tetrazine absorption band. All spectra and corresponding intensities have been normalized to the signal at $t=0$. d) Kinetic profile for the formation of pyridazine for UiO-68-TZDC compared to the H_2tzdc linker in equivalent conditions in DMF at 70 °C. Percentages of conversion were quantified by ^{1}H NMR analysis. e) DFT calculation showing the effect of reticulation in shifting the energy of the LUMO of the diene for an increase in the reaction rate.

maximum absorption for UiO-68-TZDC crystals at $t=0$ (Figures 3b,c). The decrease in intensity of the absorption maximum with time seems to follow a fast regime at short reaction times up to 180 min, where there is a decrease in the slope for slower TZDC degradation. Though the discoloration of the MOF might be considered representative of the progress of the iEDDA reaction, we chose to run another kinetic experiment that accounted for the actual formation of PZDC and provided a meaningful comparison with the reactivity of the free linker in the same conditions. We opted for reactions in DMF at 70 °C to avert the limited solubility of H_2tzdc dicarboxylic acid in ether. The amount of MOF was fixed to ensure an effective concentration of the linker in the heterogeneous solid/liquid phase equivalent to the homogeneous experiments in solution (9 mM). We quantified the product of the reaction with time by integration of the ^{1}H NMR peak area of pyridazine by using fumaric acid as an internal standard (Section S3.1). Figure 3d shows the rate of PZDC formation with time by reaction of NBD with UiO-68-TZDC or H_2tzdc. Both experiments show an exponential profile indicative of a pseudo-first order reaction with a plateau near 95 % of PZDC formation. Even though the PSM reaction must be limited by the diffusion of the dienophile the reaction proceeds much faster in the case of the mesoporous MOF. We performed an additional test in presence of $ZrCl_4$ to rule out the catalytic effect of Zr^{IV} ions as demonstrated by its negligible effect on the reaction rate for the free linker. We argue the accelerated reactivity in UiO-68-TZDC can be attributed to a sum of different reasons. Reticulation of TZDC in the framework might be certainly effective in preventing π–π stacking of the diene molecules in solution, that might disfavor reactivity. However, the key factor in controlling iEDDA reactivity between electron-deficient 1,2,4,5-tetrazines and alkenes is the energy difference between the LUMO of the first and the HOMO of the dienophile.[19] For a given alkene, electron-withdrawing substituents in the tetrazine can lower the LUMO energy for stronger interactions and higher reactivity. We used density functional theory (DFT) as implemented in VASP for analyzing the electronic effect of metal coordination in shifting the LUCO of UiO-68-TZDC, that is centered at the tetrazine linker (See Supplementary Section S3.2. for computational details). We observe a decrease in energy of 3.8 kcal mol^{-1} compared to the free linker for a narrowing of the gap between frontier orbitals and subsequent increase in the reaction rate (Figure 3e). Compared to the shift of 2.3 kcal mol^{-1} reported for di-pyridine substituted tetrazines,[20] the reticulation of the linker in the MOF seems to be more effective in lowering the LUMO energy. Although we cannot exclude the effect of free carboxylic groups in disfavoring the reactivity of free H_2tzdc, this electronic effect seems to be the most likely reason for the enhanced UiO-68-TZDC and NBD reactivity.

Encouraged by our results, we decided to illustrate the versatility of the iEDDA reaction for PSM modification of

UiO-68-TZDC with an ample range of substrates. We selected alkene and alkyne dienophiles that encompassed changes in substituents, ring strain and steric effect, all relevant to fine-tuning the $LUMO_{diene}$–$HOMO_{dienophile}$ energy gap and Diels–Alder reactivity. Our scope included a first group of alkenes as 4-(cyclopent-1-en-1-yl)morpholine, 2,3-dihydrofuran and trimethyl((1-phenylvinyl)oxy)silane and the strained cycloalkyne (1α,8α,9β)-Bicyclo[6.1.0]non-4-yne-9-methanol, all amenable to rearomatization for the generation of pyridazine (PZDC) units. This was complemented with substituted norbornenes as 5-norbornene-2-acetic acid succinimidyl ester and 5-norbornene-2-carboxylic acid and unstrained alkenes as 4-methyl-1-pentene or 1-octene, more prone to generate dihydropyridazines (HPZDC). The transformation of tetrazine linkers in functionalized PZDC or HPZDC rings was analyzed by ^{1}H NMR (Supplementary Section 4.2). Integration of the signals confirms the disappearance of the TZDC signals, and the appearance of new ones associated with the products. Suggesting a conversion rate close to 95 %, except for the unstrained dienophiles 4-methyl-1-pentene and 1-octene. This is not surprising and agrees well with the poorer reactivity documented for these non-cyclic, electron-poor molecules,[10] that would require more drastic condition or a higher number of equivalents to achieve higher yields. The formation of the iEDDA reaction products was additionally confirmed by mass spectrometry (Table S5). The CHN analysis of the crystals after evacuation of the solvent are also consistent with a clean functionalization (Table S6), that imposes small changes to the thermal stability of the functionalized frameworks according to their TGA profiles in air (Table S7). The PXRD of the crystals after PSM reaction (Figure 4a) confirmed that the crystallinity was retained in all cases with minimum impact to the original structure for a rich collection of groups decorating the mesoporous cavities of UiO-68-PZDC and HPZDC that include fused rings (CP), alkyl hydroxy (OH) and phenyl rings (Ph), succinimide (NRS) or carboxylic terminated groups (COOH), and isobutyl (*i*-Bu) or hexyl (Hex) chains, respectively. A special mention goes to UiO-68-PZDC(BCN-OH), which apart from ring-fused pyridazines and useful points of guest recognition through its -OH groups, presents stereocenters within the cavities for the generation of chiral frameworks. We selected 7 candidates to confirm the retention of porosity after PSM reaction and evacuation. All samples measured display type-I isotherms with surface areas ranging from 3100 to 1300 $m^2 g^{-1}$ (Figure 4b). We also observe a shift in the pore size of the microporous cavities that oscillate between 2.1 and 1.8 nm (Figure 4c). These changes are associated to the incorporation of bulky substituents to the framework cavities and agree well with the effect of steric crowding in the pore volume calculated from the PZDC and HPZDC framework models, that were generated computationally and analyzed with zeo++ (Figure 4d).[21]

Built upon these results, we speculated on the possibility of extending our approach to fullerene molecules for covalent conjugation to the framework. Crystalline fulleretic frameworks are interesting materials in molecular electronics, photosensitization, biomedicine or organic photovoltaics based on the combination of the excellent electron-acceptor ability, high charge mobility or broad light absorption of fullerene with the periodic order, high surface areas, chemical tunability and rich pore chemistry of reticular solids.[22] To date, the synthetic strategies to incorporate C_{60} to MOFs can be summarized into coordinative or non-coordinative immobilization. The first relies on the derivatization of fullerene with coordinating functional groups as pyridyl or carboxylate and their use as organic connectors to direct framework assembly.[23–25] This approach suffers from the intrinsic restrictions to C_{60} functionalization and the limited solubility of these molecules in the synthetic conditions conventionally used in MOF chemistry. Also, the use of soft metal ions often leads to poor framework stability toward solvent evacuation for non-permanent porosities. Non-coordinative encapsulation of

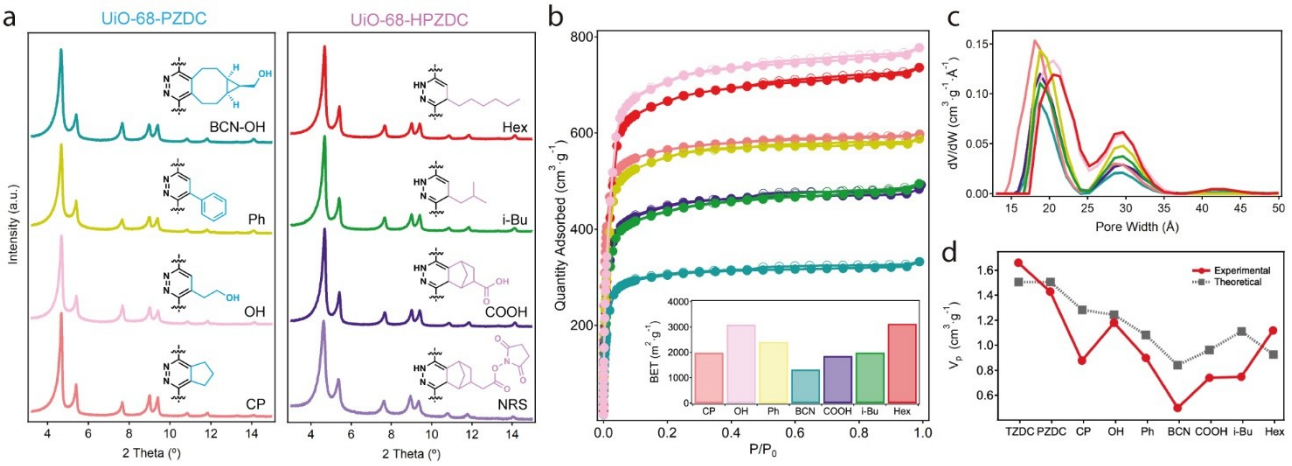

Figure 4. a) PXRD patterns of UiO-68-PZDC and HPZDC MOFs confirming minimum impact to crystallinity after iEDDA reaction in all cases. b) N_2 isotherms at 77 K and experimental BET surface areas (*inset*). c) PSD analysed by NLDFT. d) Experimental variation of pore volume with functionalization and comparison with the theoretical changes calculated from simulated crystallographic files.

fullerene guests by infiltration[26–32] or mechanochemical grinding[33] is arguable more adequate to exploit the rich variety of MOF topologies and porosity metric available. However, it suffers from diffusion limitations, which often impose poor loadings per unit cell, and the absence of specific binding sites that result in disordered guest positioning inside the pore not amenable to X-ray analysis.

We argued tetrazine linkers might be ideal plug-and-play tags for the covalent conjugation of pristine C_{60} molecules, that circumvented these limitations and enabled efficient one-step incorporation of fullerene combined with covalent anchoring for spatial control. We adapted the synthetic conditions described above to the singular solubility of fullerene (Section S5.1). UiO-68-TZDC crystals were reacted with six equivalents of commercial grade C_{60} in toluene. The mixture was incubated in a shaking oven for 3 days at 40 °C, followed by Soxhlet washing with toluene overnight, filtration and storage in hexane. The reaction induced a change in the color of the crystals from pink to brownish that was indicative of successful functionalization (Figure 5a). To rule out physical adsorption, we repeated the same reaction by using UiO-68 crystals. Thorough washing with toluene was sufficient to remove the encapsulated fullerene and revert their color to yellow, confirming the necessity of tetrazine tags for irreversible incorporation of C_{60}. The UV/Vis solid spectrum of the crystals shows a

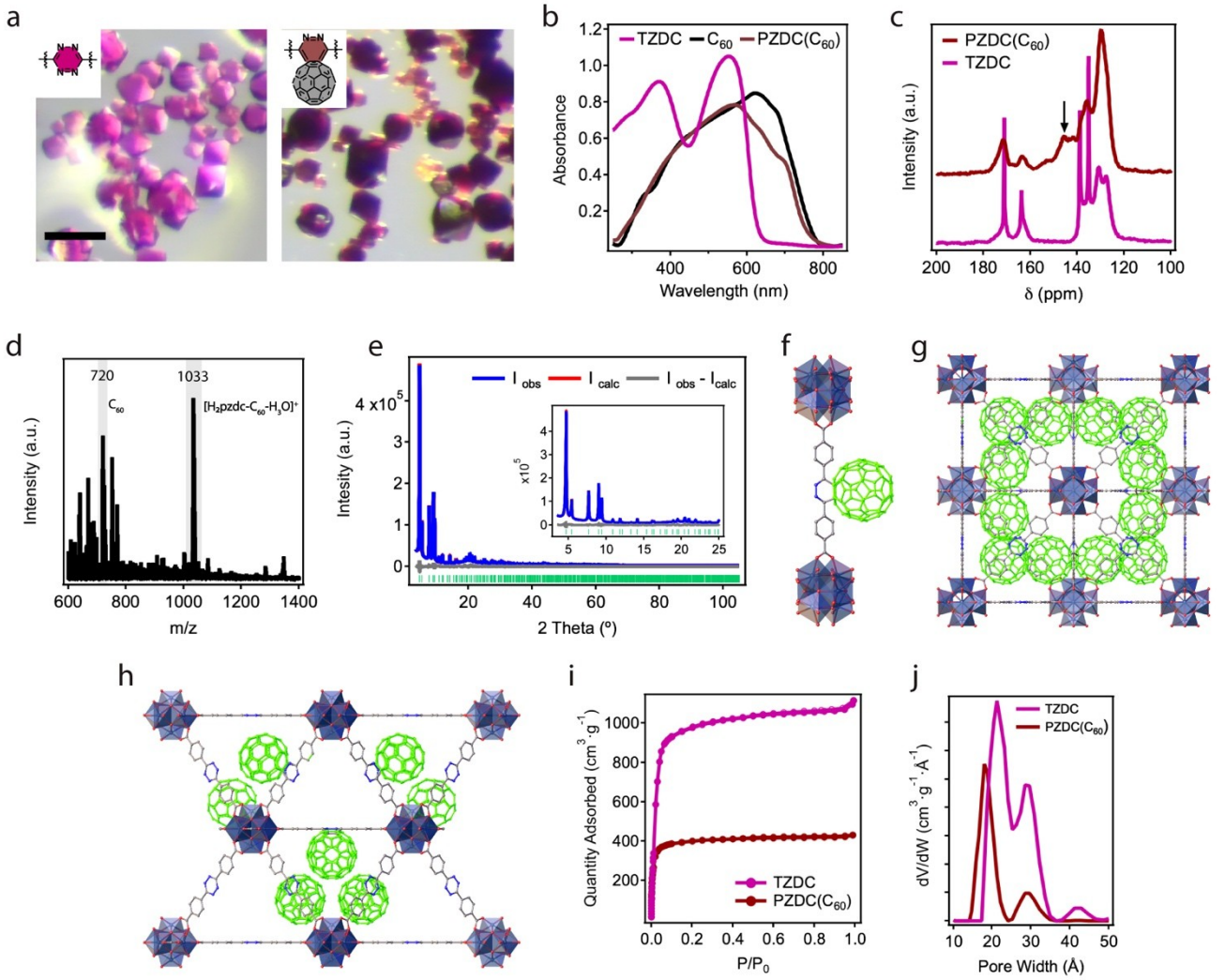

Figure 5. a) Crystals of UiO-68-TZDC before (*left*) and after (*right*) reaction with fullerene. Scale bars correspond to 50 μm. b) Solid-state UV/Vis diffuse reflectance spectra of UiO-68-PZDC(C_{60}) suggesting the incorporation of fullerene. c) Solid-state ^{13}C NMR spectra of UiO-68-TZDC and UiO-68-PZDC(C_{60}) revealing the appearance of an additional band in the sp^2 carbon region. d) Mass spectra of UiO-68-PZDC(C_{60}) crystals digested in acid. e) Experimental (blue line), calculated (red line), difference plot [($I_{obs}-I_{calc}$)] (black line, bottom panel) and Bragg positions (green ticks) for the Rietveld refinement of experimental diffraction data of UiO-68-PZDC(C_{60}) after exchange with hexane. f) View of the H_2pzdc-C_{60} units that result from the covalent grafting of fullerene (in green) to tetrazine connectors. Structure of UiO-68-PZDC(C_{60}) along g) 100 and h) 110 directions showing the distribution of fullerenes in half the tetrahedral cavities characteristic of UiO-type frameworks. Note that the symmetry was reduced from $Fm\bar{3}m$ to $P23$ for the sake of clarity. The solvent molecules and hydrogen atoms have been omitted for clarity. i) Experimental N_2 isotherms of UiO-68-TZDC and PZDC(C_{60}) at 77 K and the corresponding j) NLDFT-PSD graphs.

broad absorption band above 600 nm, that confirms the incorporation of fullerene. Comparison of UiO-68-PZDC-(C_{60}) with pristine C_{60} reveals resolved features at different wavenumbers, that suggest electronic differences in both cases (Figure 5b). Covalent conjugation to the framework was confirmed with solid-state magic angle spinning ^{13}C NMR spectroscopy (Figure 5c). Comparison of the spectra of UiO-68-PZDC(C_{60}) crystals with the parent MOF confirms the appearance of an additional band in the sp^2 carbon region. Even though it is impossible to confirm a specific symmetry for the monoadduct after the cycloaddition, the reaction of [6,6] rather than [5,6] π-bonds are expected to be more favorable from thermodynamic and kinetic standpoints.[34] Functionalization was further confirmed by mass spectrometry of the crystals after digestion in a $DMSO/H_2SO_4$ mixture (Figure 5d). The positive MALDI-TOF spectrum confirms covalent ligation of C_{60} to the tetrazine linker for hydrated monoadducts of pyridazine $[H_2pzdc\text{-}C_{60}\text{-}H_3O]^+$ linkers at $m/z = 1033$, and pristine fullerene at 720 possibly due to the molecule fragmentation upon ionization (see Supplementary Section S5.2 for further discussion). We used tandem mass spectrometry to confirm that neat fullerene molecules were generated from the fragmentation of the monoadduct and not associated to ineffective functionalization or its occlusion in the mesopores of the MOF.

Although the reaction does not impose changes to the size or morphology of the crystals, our experiments with synchrotron radiation (ALBA, BL13-XALOC) revealed very weak X-ray diffraction at resolutions higher than 1.47 Å. For better understanding of the structure of the fulleretic material, we used a structural model generated with Materials Studio as initial input for the Rietveld refinement of a high-resolution powder diffraction data set. As shown in Figure 5e, the refinement converged with excellent statistics for a cubic $Fm\bar{3}m$ space group with cell parameters $a = 32.5556(2)$ Å ($R_{Bragg} = 0.010$, $R_p = 0.033$ and $R_{wp} = 0.046$). UiO-68-PZDC(C_{60}) is isostructural to UiO-68-TZDC but displays slightly elongated cell axis and the covalent conjugation of C_{60} units to the tetrazine ring for the formation of $H_2pzdc\text{-}C_{60}$ units (Figure 5f).

The occupancy factors of fullerene molecules were refined freely to account for the total functionalization. The model converged for the formation of near to 50 % of pyridazine PZDC-C_{60} units for a crystallographic unit cell formula of $[Zr_6O_4(OH)_4(PZDC\text{-}C_{60})_3(TZDC)_3]$. A more detailed description of the structure solution can be found in the Supplementary Section S5.3. This degree of functionalization is in excellent agreement with the elemental and thermogravimetric analysis of the crystals (Section S5.2). Fullerene molecules are crystallographically disordered and, their electron density is distributed symmetrically across the solid as result of the cubic symmetry. To simplify the analysis, we reduced the symmetry to a $P23$ space group whilst retaining the net occupancy factors a clearer overview of the distribution of fullerene units. As shown in Figures 5g and 5h, UiO-68-PZDC(C_{60}) shows a regular conjugation of three C_{60} molecules to the edges of 50 % of the tetrahedral cavities that are characteristic of UiO-type frameworks. This is in excellent agreement with the accessible porosity of the crystals. The material shows a type-I isotherm for an experimental surface area of near 1700 $m^2 g^{-1}$ (Figure 5i), and retention of micro and mesoporosity at near 1.8 and 2.9 nm, respectively (Figure 5j). Even though the experimental pore volume is reduced to near 50 % compared to pristine UiO-68-TZDC (0.65 and 1.51 $cm^3 g^{-1}$, respectively), the porosity available would be in principle compatible with the loading of additional molecules, as demonstrated by the presence of solvent molecules in the as-synthesized structure.

We speculated that the loading of three molecules of C_{60} per unit cell could be fixed by the diffusion limitations imposed by the steric crowding of the pore, and the repulsive intermolecular interactions that might prevent further functionalization. To confirm this point, we synthesized alternative sets of UiO-68-PZDC(C_{60}) by extending the reaction time to 5 days. CHN and TGA data confirm very similar functionalization degrees, between 50 and 55 %, suggesting that this upper limit is controlled by steric impediments. This was corroborated with a control experiment by using multivariate UiO-68 crystals that combined reactive (TZDC) and non-reactive (TPDC) linkers. UiO-68-$TZDC_{44\%}$ was prepared according to our reported protocol,[17] and reacted with fullerene by following the conditions described above. Our results confirm complete derivatization of the tetrazine rings when diluted with terphenyl linkers, suggesting the possibility of fine tuning C_{60} incorporation in multivariate fulleretic materials (Section S5.4).

Conclusion

We have demonstrated the general value of tetrazine linkers as plug-and-play tags for general framework functionalization in one-step. The compatibility of these electron deficient linkers with the inverse Diels–Alder reaction can be considered as a rapid, highly efficient post-synthetic route for the generation of a rich diversity of pore environments. Our results also suggest that the reticulation of 1,2,4,5-tetrazine linkers in mesoporous frameworks might have an electronic effect over iEDDA reactivity with a broad range of dienophiles, which results in quantitative transformations into pyridazine and dihydropyridazine derivatives in all cases. Also important, we demonstrate how this general framework ligation scheme can be a useful tool to produce crystalline fulleretic materials. Compared to other routes, the incorporation of C_{60} is exclusively controlled by the density and distribution of tetrazine linkers in the solid, which might be an interesting alternative to control their spatial distribution and intermolecular separation for targeted function in molecular electronics or photovoltaics. Provided the compatibility of this reaction with biological applications, we are currently exploring its potential for covalent bioconjugation of enzymes to reticular solids via orthogonal iEDDA ligation chemistry.

Acknowledgements

This work was supported by the EU (ERC Stg Chem-fs-MOF 714122), the Generalitat Valenciana (PROMETEU/2021/054, SEJIGENT/2021/059 & IDIFEDER/2021/075) and the Spanish government (CEX2019-000919-M, PID2020-118117RB-I00, PID2020-113608RB-I00 & EUR2021-121999). B.L.-B. thanks the Spanish government for a FPU (FPU16/04162). N.M.P. thanks La Caixa Foundation for a Postdoctoral Junior Leader–Retaining Fellowship (ID 100010434 and fellowship code LCF/BQ/PR20/11770014). R.V. acknowledges the Programa Juan de la Cierva Formación for a postdoctoral fellowship (FJC2020-045043-I). We also thank the University of Valencia for research facilities (NANBIOSIS) and ALBA for the provision of synchrotron radiation facilities (XALOC, proposal 2021095461).

Conflict of Interest

The authors declare no conflict of interest.

Data Availability Statement

The data that support the findings of this study are available from the corresponding author upon reasonable request.

Keywords: Click Chemistry · Diels–Alder · Fullerene · Metal-Organic Frameworks · Tetrazine Tags

[1] R. Freund, S. Canossa, S. M. Cohen, W. Yan, H. Deng, V. Guillerm, M. Eddaoudi, D. G. Madden, D. Fairen-Jimenez, H. Lyu, L. K. Macreadie, Z. Ji, Y. Zhang, B. Wang, F. Haase, C. Wöll, O. Zaremba, J. Andreo, S. Wuttke, C. S. Diercks, *Angew. Chem. Int. Ed.* **2021**, *60*, 23946–23974; *Angew. Chem.* **2021**, *133*, 24142–24173.
[2] M. Kalaj, S. M. Cohen, *ACS Cent. Sci.* **2020**, *6*, 1046–1057.
[3] S. M. Cohen, *Chem. Rev.* **2012**, *112*, 970–1000.
[4] T. Kawamichi, T. Haneda, M. Kawano, M. Fujita, *Nature* **2009**, *461*, 633–635.
[5] Z. Wang, S. M. Cohen, *J. Am. Chem. Soc.* **2009**, *131*, 16675–16677.
[6] A. C. McKinlay, R. E. Morris, P. Horcajada, G. Férey, R. Gref, P. Couvreur, C. Serre, *Angew. Chem. Int. Ed.* **2010**, *49*, 6260–6266; *Angew. Chem.* **2010**, *122*, 6400–6406.
[7] A. D. Burrows, C. G. Frost, M. F. Mahon, C. Richardson, *Angew. Chem. Int. Ed.* **2008**, *47*, 8482–8486; *Angew. Chem.* **2008**, *120*, 8610–8614.
[8] Y. Goto, H. Sato, S. Shinkai, K. Sada, *J. Am. Chem. Soc.* **2008**, *130*, 14354–14355.
[9] M. Savonnet, D. Bazer-Bachi, N. Bats, J. Perez-Pellitero, E. Jeanneau, V. Lecocq, C. Pinel, D. Farrusseng, *J. Am. Chem. Soc.* **2010**, *132*, 4518–4519.
[10] A. C. Knall, C. Slugovc, *Chem. Soc. Rev.* **2013**, *42*, 5131–5142.
[11] J. Zhang, V. Shukla, D. L. Boger, *J. Org. Chem.* **2019**, *84*, 9397–9445.
[12] B. L. Oliveira, Z. Guo, G. J. L. Bernardes, *Chem. Soc. Rev.* **2017**, *46*, 4895–4950.
[13] C. Chen, C. A. Allen, S. M. Cohen, *Inorg. Chem.* **2011**, *50*, 10534–10536.
[14] L. Feng, S. H. Lo, K. Tan, B. H. Li, S. Yuan, Y. F. Lin, C.-H. Lin, S. L. Wang, K. L. Lu, H. C. Zhou, *Matter* **2020**, *2*, 988–999.
[15] M. Vinu, K. Sivasankar, S. Prabu, J. Han, C. Lin, C. Yang, J. Demel, *Eur. J. Inorg. Chem.* **2020**, 461–466.
[16] D. Jędrzejowski, M. Pander, W. Nitek, W. Bury, D. Matoga, *Chem. Mater.* **2021**, *33*, 7509–7517.
[17] B. Lerma-Berlanga, C. R. Ganivet, N. Almora-Barrios, S. Tatay, Y. Peng, J. Albero, O. Fabelo, J. González-Platas, H. García, N. M. Padial, C. Martí-Gastaldo, *J. Am. Chem. Soc.* **2021**, *143*, 1798–1806.
[18] D. A. Roberts, B. S. Pilgrim, J. D. Cooper, T. K. Ronson, S. Zarra, J. R. Nitschke, *J. Am. Chem. Soc.* **2015**, *137*, 10068–10071.
[19] F. Liu, Y. Liang, K. N. Houk, *J. Am. Chem. Soc.* **2014**, *136*, 11483–11493.
[20] W. Chen, D. Wang, C. Dai, D. Hamelberg, B. Wang, *Chem. Commun.* **2012**, *48*, 1736–1738.
[21] T. F. Willems, C. H. Rycroft, M. Kazi, J. C. Meza, M. Haranczyk, *Microporous Mesoporous Mater.* **2012**, *149*, 134–141.
[22] A. M. Rice, E. A. Dolgopolova, N. B. Shustova, *Chem. Mater.* **2017**, *29*, 7054–7061.
[23] P. Peng, F. F. Li, V. S. P. K. Neti, A. J. M. Magana, L. Echegoyen, *Angew. Chem. Int. Ed.* **2014**, *53*, 160–163; *Angew. Chem.* **2014**, *126*, 164–167.
[24] D. E. Williams, E. A. Dolgopolova, D. C. Godfrey, E. D. Ermolaeva, P. J. Pellechia, A. B. Greytak, M. D. Smith, S. M. Avdoshenko, A. A. Popov, N. B. Shustova, *Angew. Chem. Int. Ed.* **2016**, *55*, 9070–9074; *Angew. Chem.* **2016**, *128*, 9216–9220.
[25] A. Kraft, P. Roth, D. Schmidt, J. Stangl, K. Müller-Buschbaum, F. Beuerle, *Chem. Eur. J.* **2016**, *22*, 5982–5987.
[26] D. Sun, F. S. Tham, C. A. Reed, P. D. W. Boyd, *Proc. Natl. Acad. Sci. USA* **2002**, *99*, 5088–5092.
[27] H. Chae, D. Siberio-Perez, J. Kim, Y. Go, M. Eddaoudi, A. Matzger, M. O'Keeffe, O. M. Yaghi, *Nature* **2004**, *427*, 523–527.
[28] E. C. Constable, G. Zhang, C. E. Housecroft, J. A. Zampese, *CrystEngComm* **2012**, *14*, 1770–1774.
[29] H. Li, M. R. Hill, R. Huang, C. Doblin, S. Lim, A. J. Hill, R. Babarao, P. Falcaro, *Chem. Commun.* **2016**, *52*, 5973–5976.
[30] S. Goswami, D. Ray, K. Otake, C.-W. Kung, S. J. Garibay, T. Islamoglu, A. Atilgan, Y. Cui, C. J. Cramer, O. K. Farha, J. T. Hupp, *Chem. Sci.* **2018**, *9*, 4477–4482.
[31] M. Souto, J. Calbo, S. Mañas-Valero, A. Walsh, G. M. Espallargas, *Beilstein J. Nanotechnol.* **2019**, *10*, 1883–1893.
[32] S. Lo, T. Kitao, Y. Nada, K. Murata, K. Ishii, T. Uemura, *Angew. Chem. Int. Ed.* **2021**, *60*, 17947–17951; *Angew. Chem.* **2021**, *133*, 18091–18095.
[33] V. Martinez, B. Karadeniz, N. Biliškov, I. Lončarić, S. Muratović, D. Žilić, S. M. Avdoshenko, M. Roslova, A. A. Popov, K. Užarević, *Chem. Mater.* **2020**, *32*, 10628–10640.
[34] G. P. Miller, M. C. Tetreau, *Org. Lett.* **2000**, *2*, 3091–3094.

Manuscript received: June 2, 2022
Accepted manuscript online: August 16, 2022
Version of record online: September 5, 2022